Optimization of spatially localized electric fields for electron-positron pair creation

S. S. Dong, M. Chen, Q. Su, and R. Grobe

Phys. Rev. A **96**, 032120 — Published 27 September 2017

DOI: 10.1103/PhysRevA.96.032120

Optimization of spatially localized electric fields for electron-positron pair creation

S.S. Dong[(1)], M. Chen[(1)], Q. Su[(1,2)] and R. Grobe[(2)]

(1) Key Laboratory for Laser Plasmas (Ministry of Education),
Department of Physics and Astronomy, IFSA Collaborative Innovation Center,
Shanghai Jiao Tong University, Shanghai 200240, China

(2) Intense Laser Physics Theory Unit and Department of Physics
Illinois State University, Normal, IL 61790-4560, USA

Using numerical solutions to the quantum field theoretical Dirac equation, we study the electron-positron pair creation process from the vacuum due to a spatially localized supercritical electric field. By varying the spatial profile of this external field, we search for optimal field configurations that maximize the pair creation rate in the steady state. We find that for the class of pulse shapes with a single maximum and fixed total energy, the rate depends non-monotonically on the field's spatial width and it is remarkably insensitive to other characteristics of the pulse shape. It turns out that the Schwinger rate can be corrected such that it can provide analytical estimates for the threshold behavior as well as finite pulse effects with surprising accuracy.

1. Introduction

Even though it has not been experimentally observed yet, the possibility of creating an electron-positron pair from the vacuum due a supercritical external electric field is one of the most fascinating predictions of the Dirac equation [1]. In fact, there are various laboratories around the world that have invested large resources into the development of new laser sources [2] that might become sufficiently intense to break down the vacuum state and to confirm the pair creation process predicted by Schwinger [3] and others [4,5]. It is therefore important to understand better under which field configurations the yield for the pair creation process can be maximized.

There are two distinctly different mechanisms that can be responsible for the creation of particle pairs. The first one is temporally induced where the time-dependence of the external field can trigger single or multi-photon transitions that excite positive energy eigenstates of the Dirac Hamiltonian from the initially occupied states with negative energy (the Dirac sea). Here the energy (frequency) of the associated photons plays a major role that determines the yield. Recent works carried out by Kohlfirst et al. [6] as well as Hebenstreit et al. [7] have examined various means of maximizing the final pair creation yield by optimizing the *temporal* pulse shape of the electric field. They also suggested that optimal control theory could provide unique means for maximizing the yield.

The second mechanism to break down the vacuum is based on the supercriticality of an otherwise time-independent external field. If here the strength of the associated electric potential V_0 exceeds twice the rest mass energy of the electron, i.e., $V_0>2mc^2$, the states of the lower and upper energy continuum of the Dirac equation can become permanently degenerate, leading to a linear growth of the created electron-positron pairs in time, which can be characterized by a single rate. Motivated by the pioneering works for the temporal case, it seems to us that it might be beneficial for future experiments to examine also the optimal *spatial* profiles to maximize the pair creation yield. In this context we point out a recent work [8] that has suggested (in contrast to common belief) that the electrons and positrons are not necessarily created in those spatial regions where the electric field amplitude is maximal. In fact, this work has provided concrete examples of simplified situations where the pair creation rate is maximal at those spatial locations where the electric field is minimal. Equivalently, there are spatial regions within the distribution where the electric field takes its largest value but not a single electron is created there. In this vein we examine in this work if, under a fixed field energy, there are optimal spatial shapes that can maximize the pair creation yield.

The research area of constrained optimization is an important sub-branch of computational mathematics and numerous textbooks have been published on this subject [9-11]. Here typically a reward or utility function is maximized with regard to some variables in the presence of some constraints on those variables. The solution techniques are non-trivial and can vary drastically with the specific type of constraints (equality or inequality based hard constraints or penalty function based soft constraints) and involve possibly linear, quadratic or dynamic programming. In our case the corresponding objective function (the pair creation yield) is a highly nonlinear and even non-perturbative function of the parameters that characterize the external electric field configuration. It requires the numerical evaluation of the complete solution set to the Dirac equation [12,13]. It is therefore difficult for us to apply these traditional optimization techniques directly to pair creation.

The current work is organized as follows. In the second section, we briefly introduce our model system and describe the computational framework to predict the rate. In the third section, we examine the class of external field configurations that have a single maximum and show that the Schwinger rate can be corrected such that it can provide reliable analytical estimates for the optimal width of the spatial distribution. In the fourth section, we examine if two-peaked shapes can increase the pair creation yield even further. We complete this work in the last section with a brief summary and a discussion of future challenges.

2. Computational quantum field theory in one spatial dimension

The pair creation process of the electron-positron pairs can be modeled by the Dirac Hamiltonian in one spatial dimension [14]

$$H_D = c\,\sigma_1\,p + \sigma_3\,c^2 + V(x) \qquad (2.1)$$

where σ_1 and σ_3 are the two Pauli matrices and the potential V(x) models the external electric field. In our numerical simulations below we use atomic units, where three fundamental constants [amount of the electron charge, the electron mass and Planck's constant $\hbar$] are all unity by definition. As a result, the speed of light is c=137.036 a.u.

The energy eigenstates of the force-free Hamiltonian (denoted by H_0) with positive energy $w_p \equiv [c^4+c^2p^2]^{1/2}$ and momentum p in the positive (up) energy continuum are described by $H_0|u;p\rangle =$

$w_p|u;p\rangle$, whereas the negative (*d*own) continuum states fulfill $H_0|d;p\rangle = -w_p|d;p\rangle$. Their spatial representation of the two-component states is given by

$$\langle x|u;p\rangle \equiv W_p(u;x) = \eta[1,\ c\ p/(c^2+w_p)]\ \exp[ipx] \tag{2.2a}$$

$$\langle x|d;p\rangle \equiv W_p(d;x) = \eta[-c\ p/(c^2+w_p),1]\ \exp[ipx] \tag{2.2b}$$

where $\eta \equiv (2\pi)^{-1/2}\ [1+c^2p^2/(w_p+c^2)^2]^{-1/2}$ denotes the normalization factor.

The total number of created pairs can be calculated from the space-time evolved quantum field operator $\Psi(x,t)$ for the electron-positron as

$$N(t) = \sum_p \sum_{p'} |\int dx\ W_p(u;x)^*\ U(t)\ W_{p'}(d;x)\ |^2 \tag{2.3}$$

where $U(t) = \exp(-i\ H_D t)$ is the time evolution operator. From this expression, the pair creation rate is defined in the long time limit as

$$\Gamma \equiv dN(t)/dt \tag{2.4}$$

In Eq. (2.3), each state $W_{p'}(d;x)$ is evolved under the full Dirac-Hamiltonian of Eq. (2.1) and then projected on each state $W_p(u;x)$. These wave function solutions can be obtained on a space-time lattice with N_t temporal and N_x spatial grid points using a well-established fast-Fourier transformation based split-operator scheme [15-19].

Alternatively, we can calculate pair creation rate according to Hund's rule [20]:

$$\Gamma = \int dE\ T(E)\ /(2\pi) \tag{2.5}$$

where T(E) is the transmission coefficient for the incoming energy E. These are two independent ways provided by Eqs. (2.4) and (2.5) to calculate the pair creation rate. Therefore these provide reliable tests for the numerical accuracy in each simulation [21,22].

3. Singly-peaked electric field envelopes

In this section we compare the pair creation rates for the class of electric field configurations that have a single maximum. One can introduce an intensity-based spatial width such that the pair creation rate is remarkably independent of the particular shape of the spatial distribution. In Sec. 3.2 we correct the original expression for the Schwinger rate to spatially inhomogeneous fields, such that we can have analytical estimates for the optimal width.

3.1 Direct comparison of four field configurations

It is obvious that it is in principle not possible to characterize the complete class of singly peaked functions by just a single parameter. In order to nevertheless be able to examine this class of envelopes systematically, we categorize the spatial distributions according to their scaling behavior around the maximum, ranging from a constant (E_R), a linear (E_T) to a Gaussian (E_G) and squared hyperbolic secant distribution (E_S) dependence on the position x. The corresponding four spatial profiles are chosen to be centered around x=0 are therefore given by

$$E_R(x) = E_{0,R}\ U(x;-w_R/2,w_R/2) \tag{3.1a}$$

$$E_T(x) = E_{0,T}\,(1-|x/w_T|)\ U(x;-w_T,w_T) \tag{3.1b}$$

$$E_G(x) = E_{0,G}\,\mathrm{Exp}[-(x^2/(2w_G^{\,2}))] \tag{3.1c}$$

$$E_S(x) = E_{0,S}\,\mathrm{Sech}^2(x/w_S) \tag{3.1d}$$

Here U(x;a,b) denotes the generalized unitstep function that is U=1 if a<x<b and U=0 otherwise. We have chosen two fields with quadratic scaling to examine also the impact of the different scalings for large x, i.e. $E_G(x) \sim \mathrm{Exp}[-x^2]$ vs. $E_S(x) \sim \mathrm{Exp}[-x]$.

It turns out that equating the four width parameters w_R, w_T, w_G and w_S is not helpful for a systematic comparison of the four field configurations. We therefore propose here to characterize the spatial extension of these fields in a better way by introducing an effective intensity-based width σ as

$$\sigma^2 \equiv 12\,\langle (x-\langle x\rangle)^2\rangle = 12\,\{\int dx\, x^2\,\rho(x) - [\int dx\, x\,\rho(x)]^2\} \tag{3.2}$$

Here the normalized "intensity" probability is defined from the electric field as $\rho(x) \equiv E^2(x) / \int dx$

$E^2(x)$. The prefactor of 12 was chosen such that σ matches the physical extension w_R for the rectangular shape $E_R(x)$. To guarantee that all configurations have the same effective intensity width σ, the parameters w introduced above need to be scaled according to $w_R = \sigma$, $w_T = (5/6)^{1/2}\,\sigma$, $w_G = 6^{-1/2}\,\sigma$ and $w_S = (\pi^2\text{-}6)^{-1/2}\,\sigma$.

The corresponding amplitude E_0 is determined uniquely by the requirement that the total energy, defined as $\int dx\, E(x)^2 = H^2$, is the same for each field. For our four configurations this leads to the scaling of the electric field amplitude $E_0 = s\, H/\sigma^{1/2}$, where the dimensionless proportionality factors are given by $s_R^2 = 1$, $s_T^2 = 3\,(3/10)^{1/2}$, $s_G^2 = (6/\pi)^{1/2}$ and $s_S^2 = 3\,(\pi^2\text{-}6)^{1/2}/4$.

In Figure 1 we have graphed the electron-positron pair creation rate Γ as defined in the prior section as a function of the effective width σ for four fixed energies H^2. To set the scale, we have graphed the spatial width in the Figure in units of 1/c a.u. For example, this means that a width of $\sigma = 1/c$ corresponds to 3.86×10^{-13} m in mks units. The first observation is that the behavior of Γ is remarkably robust despite the rather different spatial distributions. In fact, the rates for the three fields $E_S(x)$, $E_T(x)$ and $E_G(x)$ are even hard to distinguish graphically, while the constant field $E_R(x)$ leads to a smaller rate for small values of H and surprisingly to a larger rate for large values of H. The second observation is that there is actually an optimal width in each case for which the pair-creation is maximum. Quite remarkably, the magnitude for this characteristic width σ_{opt} is rather similar for all four shapes. We will discuss the non-trivial scaling of σ_{opt} with H^2 further below. The lack of dependence of the optimal width on spatial distribution of the field also confirms that the intensity-based characterization of the spatial extension in Eq. (3.2) above was indeed physically meaningful.

There are three distinct regions depending on the value of σ. Even so it is hard to see from the Figures, for very small widths $0<\sigma<\sigma_{crit}$ we observe that Γ vanishes even though the electric field amplitude E_0 grows to infinity for $\sigma \to 0$ in order to maintain the required fixed field energy H^2. In this region, $\Gamma=0$ is expected as the amplitude V_0 of the associated electric potential, defined as $V_0 \equiv \int_{-\infty}^{\infty} dx\, E(x)$, has to exceed the well-known threshold value to permit a permanent supercritical pair-creation, i.e. $V_0 > 2c^2$. For example, for $E_R(x)$ with $E_0 = H/\sigma^{1/2}$ this supercritical width σ_{crit} amounts to $\sigma_{crit} = 4c^4/H^2$.

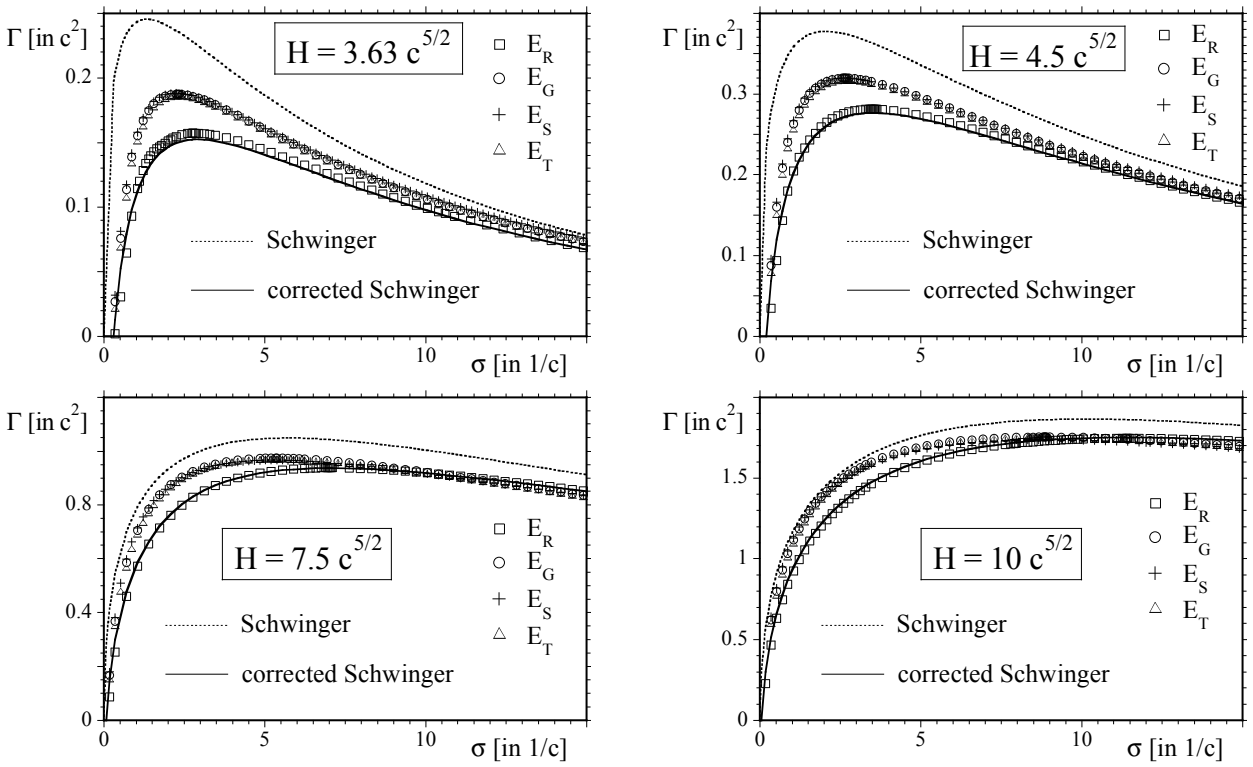

Figure 1. The steady state pair-creation rate Γ as a function of the effective width σ of four electric field configurations with a singly-peaked spatial envelope. We also denote the predictions due to the original Schwinger formula and its corrected form. (a) H=3.63 $c^{5/2}$, (b) H=4.5 $c^{5/2}$, (c) H=7.5 $c^{5/2}$, (d) H=10 $c^{5/2}$.

The second region $\sigma_{crit}<\sigma<\sigma_{opt}$ is characterized by a monotonic increase of the rate Γ with σ. This region marks the onset of the supercritical pair-creation process, for which the rate Γ naturally has to increase with σ.

In the third region $\sigma_{opt}<\sigma<\infty$, the rate decreases again. This decrease is expected as a result of two competing mechanisms. If we take $E_R(x)$ as an example, we find that the associated height of the potential V_0 grows only weakly with σ as $V_0 = H\,\sigma^{1/2}$. On the other hand, the spatial extension of the region where the potential grows from 0 to V_0 increases with σ as well. As an increasing extension is directly associated with a larger tunneling distance, which typically decreases the transmission coefficient for an incoming electron [see Eq. (2.5)], this mechanism decreases the pair creation [8] and apparently dominates the other effect for large σ. Additionally, in order to maintain the fixed energy, the electric field amplitude $E_{0,R} = H\,\sigma^{-1/2}$ decreases as the pulse gets wider, which also suggests a decreasing rate Γ.

3.2 The correction of the Schwinger rate for finite narrow static spatial distributions

The spatial profile of the pulse for $E_R(x)$ characterizes a spatial region where the electric field is uniform. For the limiting case of an infinitely extended electric field Schwinger's well-known rate formula [3] should become valid. In one spatial dimension [23], it predicts that the creation rate per unit length is given by $(E_0/2\pi)\,\mathrm{Exp}[-\pi c^3/E_0]$. We should remind the reader that this expression is highly-nonperturbative in E_0 and can be derived using Borel summation techniques of a diverging perturbative expansion [24]. To have an approximate but analytical estimate, we can loosely interprete $\Gamma_{\mathrm{Schwinger}} \equiv \sigma\,(E_0/2\pi)\,\mathrm{Exp}[-\pi c^3/E_0]$ as the prediction of the Schwinger formula for a rectangular pulse of extension σ. This rate increases linearly with the width σ. To the best of our knowledge, with a few exceptions, systematic studies that examine the validity of the Schwinger formula for fields with a finite extension are lacking. As we use the Schwinger formula for several approximate scaling estimates below, we therefore need to establish its validity in the finite pulse regime first.

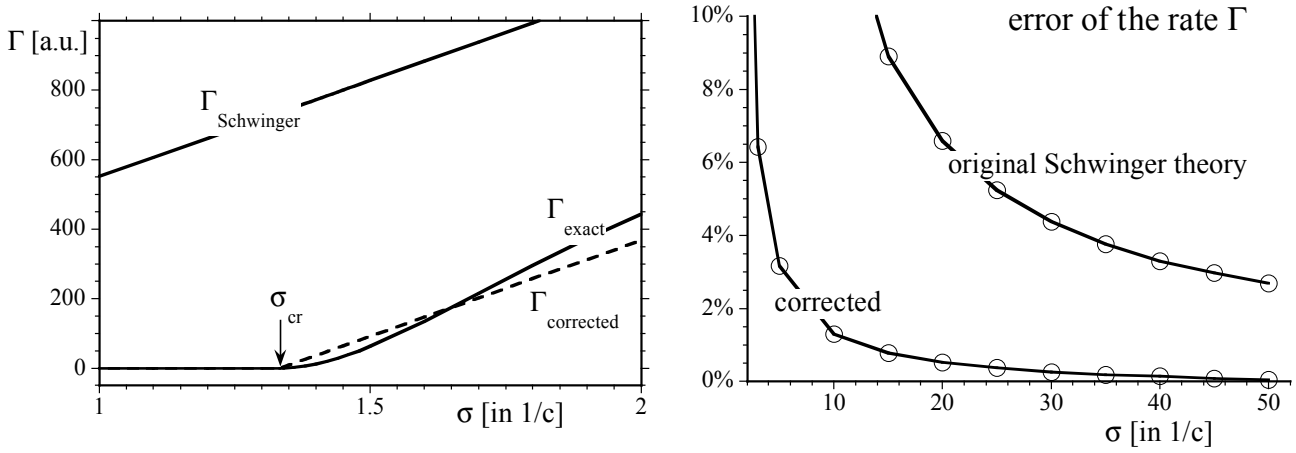

Figure 2. (a) Comparison of the prediction of the Schwinger formula for the steady state pair-creation rate $\Gamma_{\mathrm{Schwinger}}$ as a function of the width σ of electric field and the exact rate Γ_{exact} for $E_0=1.5c^3$. (b) The percentage error of the original Schwinger rate together with the error associated with the corrected Schwinger expression.

In Figure 2 we compare the Schwinger rate $\Gamma_{\mathrm{Schwinger}}$ with the exact one Γ_R obtained from the rectangular pulse $E_R(x)$ for a fixed electric field $E_0 = E_{0,R} = 1.5c^2$. As expected, we find that the two rates become similar for very large widths σ, while the Schwinger rate remains consistently

larger than the exact one. This means that the original Schwinger rate overestimates the true rate for any width. For example, for σ=5/c the relative error between both is 32% and decreases to less than 2.7% for σ=50/c as shown in Fig. 2b. However, for small widths σ the Schwinger rate significantly overestimates the rate. In fact, the true rate Γ_R is only non-zero once the associated potential becomes supercritical, i.e., $E_{0,R}\,\sigma > 2c^2$. This leads to a critical width $\sigma_{cr} \equiv 2c^2/E_{0,R}$ below which the rate is zero. In contrast, the (infinite width-based) Schwinger rate would predict $\Gamma_{Schwinger} = c^2/\pi\ Exp[-\pi c^3/E_0]$ at this particular width instead of the correct value of zero. This nonvanishing value of $\Gamma_{Schwinger}$ is related to the nearly constant offset between $\Gamma_R(\sigma)$ and $\Gamma_{Schwinger}(\sigma)$ as indicated in the Figure 2a. In order to correct the Schwinger expression for this finite-width effect, we can simply subtract this offset and therefore introduce a new rate defined as

$$\Gamma_{cor} \equiv [\sigma\, E_0/2 - c^2]/\pi\ \ Exp[-\pi c^3/E_0] \qquad (3.3)$$

This new rate becomes positive only if the field is supercritical and also naturally corrects the offset shown in Figure 2a. We had included the original Schwinger prediction as well as the corrected rate already in the Figure 1. We find that the corrected rate Γ_{cor} matches the true rate for rectangular pulses $E_R(x)$ for the entire range of the widths as well as all pulse energies displayed.

In order to be more quantitative, we show in Figure 2b that the corrected Schwinger rate can approximate the true rate with significantly less relative error (defined as $|\Gamma-\Gamma_{exact}|/\Gamma_{exact}$) than the one from the original expression. For example, the corrections to the Schwinger formula are significant improvements as they decrease the errors cited above from 32% to only 3.1% (for a small width σ=5/c) and from 2.7% to 0.5% (for a large width σ=50/c).

After we have established the accuracy of the corrected Schwinger rate even for electric fields with relatively small extensions, we can now use the analytical expression to analyze the scaling behavior of the rate as well as the optimal width for the class of pulses with fixed energy. If we use again $E_0 = H/\sigma^{1/2}$, the analytical rate becomes

$$\Gamma_{cor}(\sigma,H) \equiv [H\,\sigma^{1/2}/2 - c^2]/\pi\ \ Exp[-\pi c^3\sigma^{1/2}/H] \qquad (3.4)$$

We can therefore use this reliable but approximate analytical expression to examine the scaling of

the optimal width. From the condition $d\Gamma_{cor}(\sigma,H)/d\sigma=0$, we find

$$\sigma_{opt} = (H^2+2c^5\pi)^2/(c^6H^2\pi^2) \qquad (3.5)$$

This means that the (corrected) Schwinger based approximation suggests that there might not be an energy independent universal optimal electric field shape. The fact that the optimal width does depend on the energy of the pulse exemplifies the true nonlinear nature of the pair creation process. In fact, for large pulse energies ($H^2>2c^5\pi$) the optimum pulse width increases with the energy, $\sigma_{opt} = H^2/(c^6\pi^2)$, whereas for small pulse energies ($H^2<2c^5\pi$), it decreases as $\sigma_{opt} = 4/(cH^2)$. It is also interesting to note that for any fixed energy H^2 the corresponding optimal pulse is supercritical. This can be seen if we compute the potential as $V_{opt} = E_0\, \sigma_{opt} = H\, \sigma_{opt}^{1/2} = H\, [(H^2+2c^5\pi)^2/(c^6H^2\pi^2)]^{1/2}$, which takes the supercritical value $V_{opt} = 2c^2$ for H=0.

If we insert the optimum width into the rate, we find that maximum rate itself grows monotonically with the energy H^2 as one could expect

$$\Gamma_{opt}(H) \equiv \Gamma_{cor}(\sigma_{opt},H) = [H^2/(2\pi^2c^3)\, Exp[-1 - 2\pi c^5/H^2] \qquad (3.6)$$

These findings predict that the maximum pair-creation rate $\Gamma_{opt}(H) \sim H^2$ would increase more rapidly with H than the usual (non-perturbative) growth of $\Gamma(H)$ for a fixed extension, i.e. $\Gamma(H) \sim H\, Exp[-\beta/H]$.

In order to examine whether this prediction also holds more generally for other configurations, we compare in Figure 3 the Schwinger prediction for σ_{opt} and Γ_{opt} with those associated with our pulse shapes introduced in Eq. (3.1). To obtain these data for the four fields was computationally quite involved as it required the computation of the entire width dependence of the rate, then finding its optimal width for each graph and then repeating these calculations for each energy.

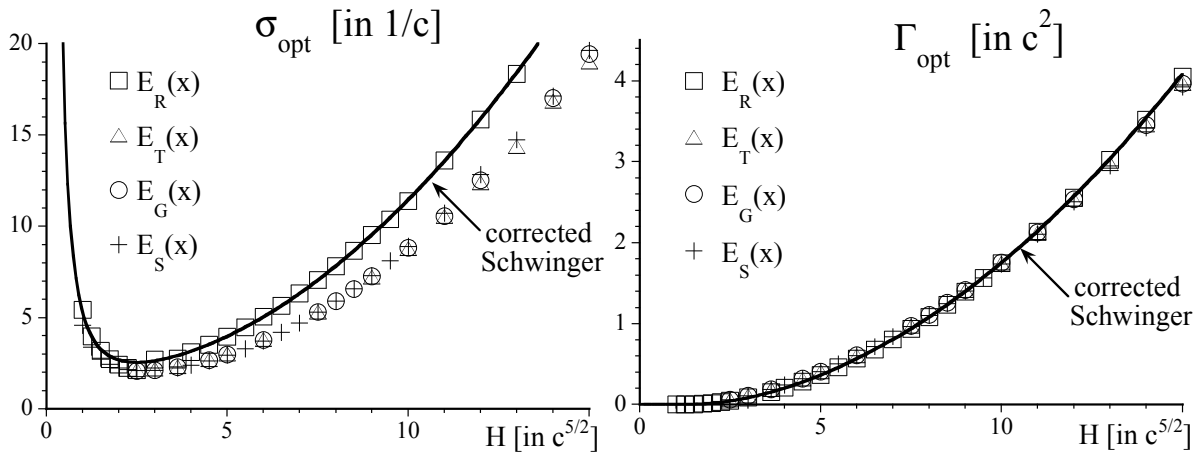

Figure 3. The optimal effective width σ_{opt} (a) and the maximal pair creation rate Γ_{opt} (b) as a function of the total energy H of the external electric field pulse.

Despite the fact that the original Schwinger rate is strictly valid only in the (unrealistic) limit of an infinitely extended electric field, the quantitative predictions for the optimal spatial width based on the corrected Schwinger formula are remarkably accurate and match the data [especially for $E_R(x)$] very well. In agreement with the other three field configurations, the data suggest that in order to maximize the yield with a singly peaked electric field configuration, the spatial extension should always exceed a minimum width of about σ=2.5/c. Furthermore, if the experimentally achievable energy H^2 is not too large, then a significantly larger spatially extended field would be ideal. In fact, the smaller this available field energy, the larger should be the spatial extension to increase the efficiency of the pair creation process. The magnitude of the maximal achievable rate (shown in Figure 3b) grows monotonically with H^2. The match of all data suggests that the simple analytical expression Eq. (3.6) is even valid for any singly-peaked electric field configuration.

4. Doubly-peaked electric field envelopes

In the last section we saw that for the class of singly-peaked envelopes there are two competing mechanisms that determine the final rate. Examining the more general class of electric field shapes with two peaks provides us with an additional degree of freedom to control the pair creation yield. Furthermore, it leads to yet another mechanism to affect the particle yield. This

mechanism is associated with the observation that the rate seems to decrease universally with increasing spatial separation of the two peaks. As we will discuss below the simultaneous presence of all three competing mechanisms can lead to the occurrence of new structures involving new local and global maxima for the rate as a function of the effective width σ of these configurations. Additionally, the new degree of freedom might also permit us to examine the question whether this new class of pulse shapes can enhance the creation rate compared to the single-peaked shapes.

In Figure 4 we have graphed the rate Γ as a function of the separation d between two rectangular fields of width w each. In the inset the corresponding electric field $E_{TP}(x) = E_R(x) + E_R(x-w-d)$ is depicted.

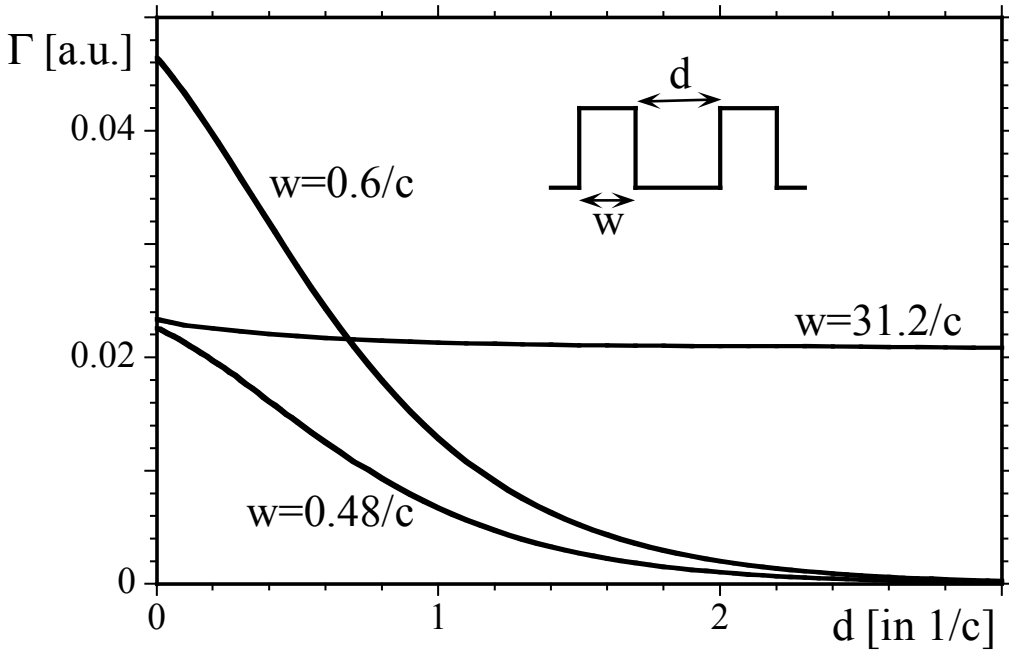

Figure 4. The steady state pair-creation rate Γ as a function of the separation d of the two electric field with the width w each. In the inset we sketch this spatial profile. The graphs correspond to the widths $w_1=0.48/c$, $w_2=0.6/c$ and $w_3=18\sqrt{3}/c$ and $H=3.63\ c^{5/2}$ and total energy $H=3.63\ c^{5/2}$.

The monotonic decrease of the rate Γ with d shows that, even though an overall extension increases the effective width σ, the rate decreases. However, the width of each single pulse w still determines the overall magnitude of the rate as the comparison of the three curves for $w_1=0.48/c$, $w_2=0.6c$ and $w_3=31.2/c$ shows. In fact, if we choose the optimum width σ_{opt} (as predicted in the prior section for a singly-peaked field) the yield is also maximum for the two-peaked configuration. The data in

Figure 4 were obtained for the same energy as those in Figure 1a, for which the yield for w_2=0.6c was also consistently larger than that for the smaller and large widths, w_1=0.46c and w_3=31.2/c, respectively. The monotonic decrease of the data with d gives us also a first indication that a singly-peaked electric field (d=0) might be more efficient for pair creation than any doubly peaked one (d≠0).

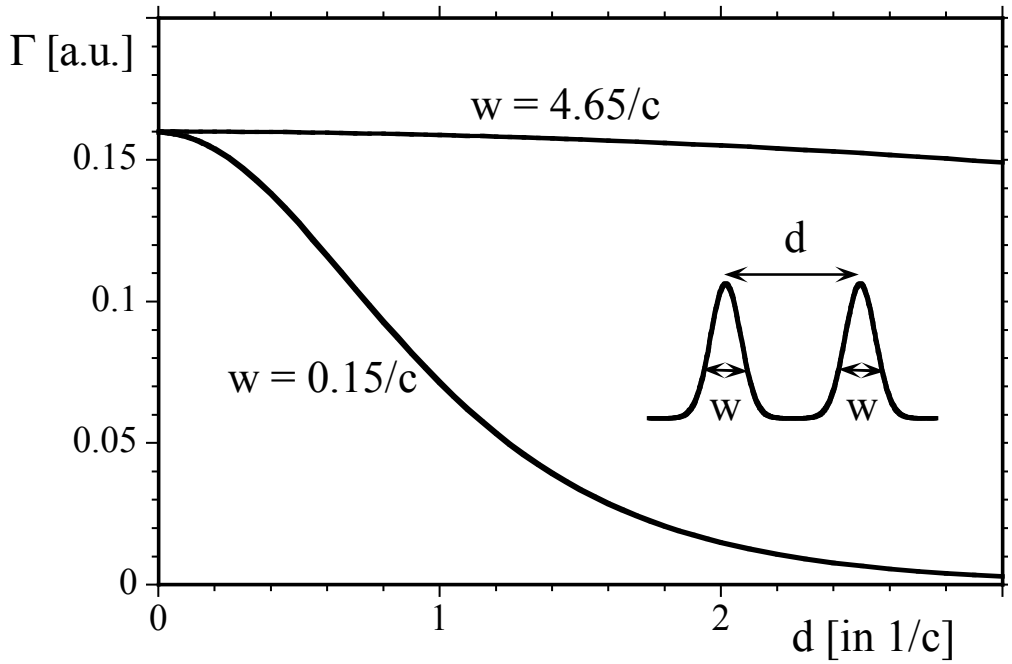

Figure 5. The steady state pair-creation rate Γ as a function of the separation d of the two electric field with a Gaussian spatial envelope and width w each. In the inset we sketch this spatial profile. The graphs correspond to width w_1=0.15/c, w_2=4.65/c and H=4.5 $c^{5/2}$.

One could conjecture that this monotonic decrease of Γ with d may not be generally true and only occurred for our particular field $E_{TP}(x)$, where the gap between the peaks vanished identically for any d≠0. To generalize this finding we have repeated the same simulation for two Gaussians, where a minimum occurs between the two pulses only if d is larger than d=2. While the electric field at this minimum decreases with d, it is never equal to zero. As we show in Figure 5, the monotonicity of the rate with d seems indeed to be rather universal. This suggests that the additional freedom of choosing electric fields with two peaks does not necessarily lead to enhanced pair creation rates. Therefore, the optimal electric field configuration is likely to be singly peaked.

Finally, we will demonstrate how the simultaneous action of the three different competing mechanisms, which are (1) the increase of Γ with σ for small σ, (2) the decrease of Γ with σ for

large σ and finally (3) the general decrease of Γ with d can lead to interesting substructures in the rate. To illustrate this we have chosen the two-peaked configuration

$$E_{TP}(x) = E_{0,R}\ U(x;-s/2,s/2) + E_{0,R}\ U(x-2s;-s/2,s/2) \qquad (4.1)$$

where the spacing s between the two fields was chosen to be equal to the extension of each peak.

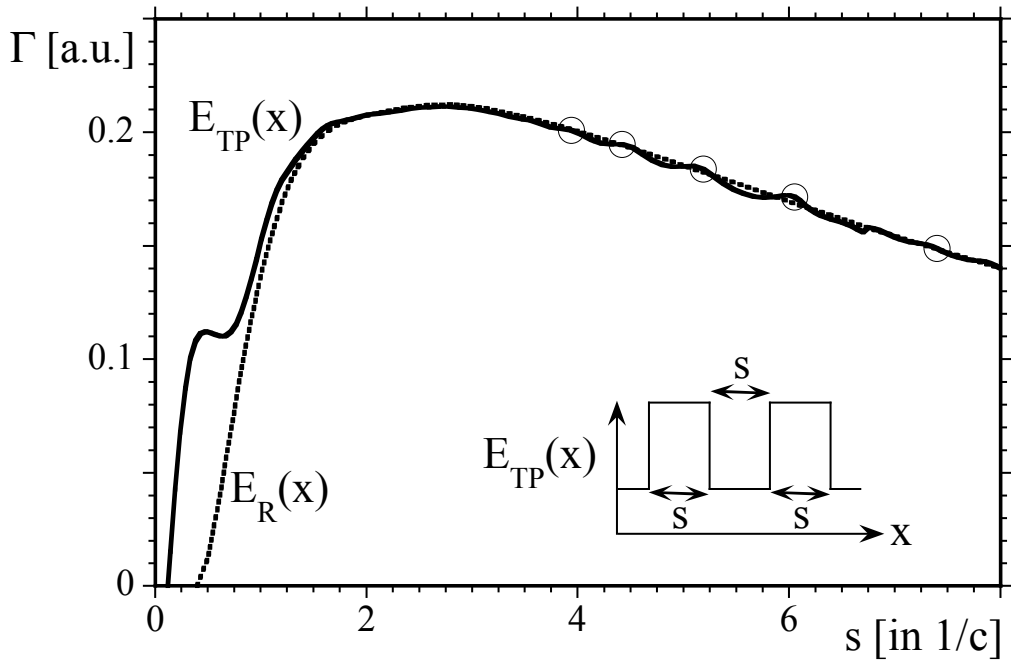

Figure 6. The steady state pair-creation rate Γ as a function of the separation s (as well as the extension s of each pulse) between the two fields. The corresponding configuration is shown in the inset. For comparison, the dashed curve is twice the rate associated with only the first pulse. The open circles are the locations of the maxima according to $s_n=33.3c^{-1}(n+1/2)^{-1}$ for n=4,5,6,7 and 8. [$H=4.5c^{5/2}$]

As the strength of each mechanism depends on s, there are four interesting regions. In agreement with Figure 1, there is the zero-production regime which is followed by the small-s growth domain. The interesting new regime is the third one where after a local maximum the rate Γ decreases and then continues to increase again. This domain of s between the local maximum and minimum of Γ is due the mechanism illustrated above in Figure 4 where any increase of the extension d of the interpulse gap region always leads to a decrease of Γ. In this region, this decreasing mechanism (3) is dominant over the "Γ increase mechanism for small-σ" (1).

The data allow us also some insight into the length scale on which the particles created by

each field pulse can affect each other. For a comparison, we have also included in the Figure twice of the rate obtained from just one of the two pulses. This would correspond to the true rate if the two pulses were infinitely apart, such that the creation of the particles in one pulse would not interfere with the generation of the pairs in the other neighboring pulse. For separations that exceed s=2/c the two graphs are indeed very similar. For small separations s, however, we observe that the rate of the two-field configuration exceeds that rate 2Γ (associated with just one pulse). Also, this difference is expected as the single pulse was chosen to have only half of the pulse energy [$H^2=(4.5\ c^{5/2})^2/2$] of the two-pulse combination. As a result, the corresponding threshold width s for pair-creation for the single pulse requires a larger width as observed in the Figure. This therefore explains that for smaller width the two-pulse combination actually leads to a larger rate.

As a side issue, we note some oscillatory structures [25] in the graph for $\sigma>6/c$. As an interplay of several length scales such as the spacing s and the de Broglie wave length of the created particles can play a role to determine the total rate, these oscillations might be the result of some destructive and constructive quantum interferences. While we have not been able to derive a phenomenological model that can predict the locations of the maxima and minima, we found that the numerical expression $s_n\ (n+1/2) = 33.3/c$ describes the actual locations of the maxima s_n remarkably well. In the graph we have indicated these predicted locations for n=4,5,6,7 and 8 by the open circles.

5. Estimation of optimal pulse shapes based on physical mechanisms

All of the estimates had to be restricted to only specific subclasses of electric field envelopes. They were optimized with regard to only a single parameter such as the width or the peak to peak spacing. This restriction was unfortunately required for computational reasons. In this section we will examine if two physical mechanisms can be used to predict a more general optimal pulse shape. We will test the Schwinger rate expression and show that it predicts $E_R(x)$ as the optimum field. Remarkably, the same pulse shape is also predicted by a classical mechanical mechanism that is based on the minimization of the particles' occupation time of the pair creation zone.

5.1 Schwinger mechanism

Despite the fact that Schwinger's special case is strictly valid only for infinitely extended configurations we have suggested above that it can provide us with some qualitative predictions

about the scaling of the optimum width. It is therefore tempting to examine whether we can apply the usual variational calculus techniques directly to find an optimum shape based on Schwinger's rate based formula. We could assume that the electric field in the rate formula is actually spatially dependent and attempt to construct the pulse shape E(x) that optimizes the spatially integrated rate given by $\Gamma \equiv \int_{-w/2}^{w/2} dx\, E(x)/(2\pi)\, Exp[-\pi c^3/E(x)]$ under the constraint $H^2 \equiv \int_{-w/2}^{w/2} dx\, E(x)^2$.

It turns out that any functional of the general form $\Gamma[E(x)] \equiv \int_{-w/2}^{w/2} dx\, f[E(x)]$ for arbitrary functions f is always optimized by a homogeneous field E(x)=const. Due to the absence of any derivative terms (such as dE/dx) the corresponding Euler-Lagrange equation is simply an algebraic equation for E(x), such as $\partial f/\partial E - \lambda\, 2E(x) = 0$, where λ is the Lagrangian multiplier. Therefore this approach does not predict any non-trivial envelope E(x) and the optimum field is given by $E_R(x)$ defined in Eq. (3.1a). This is consistent with the case for very large field energies H^2 (compare Figure 1d), where we also observed that for large σ the constant-field pulse E_R led to a larger pair creation rate than the other three inhomogeneous fields E_G, E_S and E_T.

The same conclusion also follows from the commutativity of the summation terms of the finite Rieman sum representation of the integral $\Gamma = \Delta x\, \Sigma\, f[E(x_n)]$. Here the summation is unchanged if we exchange the values of the function at arbitrary locations x_N and x_M, i.e. $E'(x_N) = E(x_M)$ and $E'(x_M) = E(x_N)$. This leads to the new function $E'(x_n) \equiv E(x_n)\, (1-\delta_{nN})\, (1-\delta_{nM}) + E(x_M)\, \delta_{nN} + E(x_N)\, \delta_{nM}$ for which $\int_{-w/2}^{w/2} dx\, f[E'(x)] = \int_{-w/2}^{w/2} dx\, f[E(x)]$. If we assume that the function $E_{opt}(x)$ that extremalizes the integral $\int_{-w/2}^{w/2} dx\, f[E_{opt}(x)]$ is unique, then this "swapping-symmetry" would permit us to construct an infinite set of equivalent functions all of which would lead to the precisely the same extremal integral, in direct contradiction to the assumed uniqueness of $E_{opt}(x)$. Therefore the optimizing function must be invariant under any swapping operation, which is true only for homogeneous fields $E_{opt}(x)$=const.

5.2 Classical mechanical occupation time

In several studies it was suggested that those electron-positron pairs that cannot leave the creation region decrease the overall pair creation process due to Pauli blocking [26-32]. Other studies [33] have suggested that some aspects of the quantum field theoretical pair creation processes such as energy spectra can be understood in terms of classical mechanics. We therefore examine here whether the time a created electron would require to accelerate out of the pair creation

zone is related to the production rate. In other words, we assume here that those electric field pulses that minimize the average occupation time of the particles in the pair creation zone can also maximize the yield.

We assume the electric field pulse localized x=0 and x=1 is modeled by an unknown potential V(x). For simplicity we assume that the particle is created at location x=0 with a total particle's total energy $V(0)=V_0$. In other words, the particle is assumed to start with zero speed and accelerates downward to the bottom of the potential at x=1, where V(x=1)=0. The total time the particle requires to travel from x=0 to x=1 is given by

$$T = \int_0^1 dx \,/\, [\, 2\,(V_0 - V(x)\,)\,]^{1/2} \tag{5.1}$$

where the potential V(x) is subject to the same constraint as used above to fix the pulse energy:

$$H^2 = \int_0^1 dx\, [dV(x)/dx]^2 \tag{5.2}$$

Note that this is not the same as the famous brachistochrone problem where the force is constant and points strictly downward but the particle accelerates in another direction. If we use a Lagrange multiplier λ and apply the first variational derivative we obtain

$$\delta\, \{\, \int_0^1 dx \,/\, [\, 2\,(V_0 - V(x)\,)\,]^{1/2} - \lambda \int_0^1 dx\, [dV(x)/dx]^2 \} = 0 \tag{5.3}$$

We arrive at the Euler–Lagrange equations for the optimum potential,

$$\partial/\partial V\ \{1/[\, 2(V_0 - V(x)\,)\,]^{1/2}\,\} + 2\lambda\, d^2/dx^2\, V(x) = 0 \tag{5.4}$$

When this equation is solved numerically together with the constraint of Eq. (5.2), we find that the potential that minimizes the time of travel in this interval is very closely approximated by $V(x) \approx V_0(1-x)$, corresponding to an electric field that is constant. Note that this conclusion is in agreement with the optimum field discussed in the previous section. The maximization of the Schwinger rate seems to be equivalent to the minimization of the occupation time of a classical particle accelerating in a constant electric field. One could have expected that those electric force

fields that are largest close to the starting point x=0 (and therefore can accelerate the particle at early times) would minimize the passage time. However, it also seems to be important that the time (and therefore the distance) over which the particle can accelerate has to be as large as possible as well in order to minimize the total passage time from x=0 to x=1. Apparently a spatially constant force field is the best compromise for these two competing requirements.

6. Summary and outlook

In this work we have shown that for the class of supercritical electric field distributions with a single peak the electron-positron pair rate is rather insensitive to the particular spatial profile. For spatial distributions with a fixed electric field energy the pair creation yield does not vary as a monotonic function of the width of the electric field. In fact, there is an optimum spatial width for each energy for which the pair creation rate is maximum. For small energies this optimal width decreases first and then increases again as the field energy is increased. We have also corrected the original Schwinger rate to account for effects due to finitely extended fields. This corrected rate provides fully analytical estimates for the optimum width as well as for the obtainable maximum pair creation yield. These analytical predictions are surprisingly accurate for a wide class of electric field configurations with a single maximum. A generalization of the simulations for spatial profiles with two maxima did not lead to an enhancement of the pair creation yield. In fact, our studies suggest that a remarkably simple spatial distribution with a structureless constant electric field is actually rather close to the optimal configuration. This surprising finding is also consistent with results based on variational principle with suitable constraints. The current work is just an initial attempt to a conceptually and also computationally difficult problem and we hope that it can stimulate further more detailed investigations.

In this work we reported mainly on field configurations that are spatially symmetric. For asymmetric electric field distributions our preliminary computations reveal that they mostly produce fewer pairs than the corresponding symmetric distributions even though they add yet another degree of freedom in searching for optimal field configurations.

Even though the pair creation process can happen on very short time scales for which even the electric and magnetic field components of an electromagnetic radiation pulse (such as an optical laser pulse) may appear time-independent, temporal characteristics of the experimentally relevant fields can also affect the pair creation process. It might be therefore worthwhile to include also temporal variations into the external field and to optimize the space-time profile. We will leave

these challenges to follow up investigations.

Our work was based on the optimization of the asymptotic long-time rate of the permanent pair creation regime. However, these asymptotic regions could be difficult to be established with the planned laser sources, where transient effects might dominate the process. Also, any radiative back reaction by the created particles on the fields was neglected in our studies. While there have been some recent promising proposals to include these effects [32,34], fully three-dimensional simulations that incorporate these interactions on a field theoretical and non-phenomenological level are very challenging. There are certainly many other promising computational and analytical approaches that can contribute to these questions, such as the Dirac–Heisenberg– Wigner formalism [35,36], worldline instantons [37,38] or real-time lattice gauge theory [39].

Acknowledgements

We thank Dr. Q.Z. Lv for many helpful discussions. This work has been supported by the NSF and the NSFC (#11128409). It also used the Extreme Science and Engineering Discovery Environment (*XSEDE*), which is supported by the NSF grant OCI-1053575.

References

[1] For a recent review, see, e.g., A. Di Piazza, C. Müller, K.Z. Hatsagortsyan and C.H. Keitel, Rev. Mod. Phys. 84, 1177 (2012).

[2] For high power laser systems, see, for example, the web sites of the following labs: ELI (Paris), diocles (Lincoln), xfel (Hamburg), sparc (Darmstadt), Vulcan, HiPER and Astra Gemini (Oxfordshire), polaris (Jena) or Shenguang III (Mianyang).

[3] J.S. Schwinger, Phys. Rev. 82, 664 (1951).

[4] F. Sauter, Z. Phys. 69, 742 (1931).

[5] W. Heisenberg and H. Euler, Z. Phys. 98, 714 (1936).

[6] C. Kohlfürst, M. Mitter, G. von Winckel, F. Hebenstreit and R. Alkofer, Phys. Rev. D 88, 045028 (2013).

[7] F. Hebenstreit and F. Fillion-Gourdeau, Phys. Lett. B 739, 189 (2014).

[8] Q.Z. Lv, J. Unger, Y.T. Li, Q. Su and R. Grobe, Euro. Phy. Lett. 116, 40003 (2016).

[9] W. Sun and Y.X. Yuan, "Optimization theory and methods: nonlinear programming (Springer, 2010).

[10] J.J. Leader, "Numerical analysis and scientific computation" (Addison Wesley, 2004).

[11] R. Dechter, "Constraint processing" (Morgan Kaufmann, Burlington, 2003).

[12] W. Greiner, B. Müller and J. Rafelski, "Quantum electrodynamics of strong fields" (Springer Verlag, Berlin, 1985).

[13] For a review, see, e.g., T. Cheng, Q. Su and R. Grobe, Contemp. Phys. 51, 315 (2010).

[14] B. Thaller, “The Dirac equation” (Springer, Berlin, 1992).

[15] J.A. Fleck, J.R. Morris and M.D. Feit, Appl. Phys. 10, 129 (1976).

[16] A.D. Bandrauk and H. Shen, J. Phys. A 27, 7147 (1994).

[17] J.W. Braun, Q. Su and R. Grobe, Phys. Rev. A 59, 604 (1999).

[18] G.R. Mocken and C.H. Keitel, Comp. Phys. Commun. 178, 868 (2008).

[19] M. Ruf, H. Bauke, and C.H. Keitel, J. Comp. Phys. 228, 9092 (2009).

[20] F. Hund, Z. Phys. 117, 1 (1941).

[21] T. Cheng, M. Ware, Q. Su and R. Grobe, Phys. Rev. A 80, 062105 (2009).

[22] Q.Z. Lv, A.C. Su, M. Jiang, Y.J. Li, R. Grobe and Q. Su, Phys. Rev. A 87, 023416 (2013).

[23] T. Cheng, Q. Su and R. Grobe, Phys. Rev. A 80, 013410 (2009).

[24] G. Dunne and T. Hall, Phys. Rev. D 60, 065002 (1999).
[25] M. Jiang, Q.Z. Lv, Z.M. Sheng, R. Grobe and Q. Su, Phys. Rev. A 87, 042503 (2013).
[26] A. Hansen and F. Randal, Phys. Scr. 23, 1036 (1981).
[27] B. R. Holstein, Am. J. Phys. 66, 507 (1998).
[28] N. Dombey and A. Calogeracos, Phys. Rep. 315, 41 (1999).
[29] B. R. Holstein, Am. J. Phys. 67, 499 (1999).
[30] P. Krekora, Q. Su, and R. Grobe, Phys. Rev. Lett. 92, 040406, (2004).
[31] P. Krekora, Q. Su and R. Grobe, Phys. Rev. A 72, 064103 (2005).
[32] A.T. Steinacher, R. Wagner, Q. Su and R. Grobe, Phys. Rev. A 89, 032119 (2014).
[33] N. Chott, Q. Su and R. Grobe, Phys. Rev. A 76, 010101 (2007).
[34] F. Hebenstreit, J. Berges and D. Gelfand, Phys. Rev. Lett. 111, 201601 (2013).
[35] I. Bialynicki-Birula, P. Gornicki and J. Rafelski, Phys. Rev. D 44, 1825 (1991).
[36] F. Hebenstreit, R. Alkofer and H. Gies, Phys. Rev. Lett. 107, 180403 (2011).
[37] H. Gies and K. Klingmüller, Phys. Rev. D 72, 065001 (2005).
[38] G.V. Dunne and C. Schubert, Phys. Rev. D 72, 105004 (2005).
[39] F. Hebenstreit, J. Berges and D. Gelfand, Phys. Rev. D 87, 105006 (2013).